8-2009

# Strain relaxation in Si/Ge/Si nanoscale bars from molecular dynamics simulations

Yumi Park
*Purdue University - Main Campus*, park201@purdue.edu

Hasan Atkulga
*Purdue University - Main Campus*

Ananth Y. Grama
*Purdue University*, ayg@cs.purdue.edu

Alejandro Strachan
*Purdue University - Main Campus*, strachan@purdue.edu

# Strain relaxation in Si/Ge/Si nanoscale bars from molecular dynamics simulations

Yumi Park,[1] Hasan Metin Atkulga,[2] Ananth Grama,[2] and Alejandro Strachan[1,3,a)]
[1]*School of Materials Engineering, Purdue University, West Lafayette, Indiana 47907, USA*
[2]*Department of Computer Science, Purdue University, West Lafayette, Indiana 47907, USA*
[3]*Birck Nanotechnology Center, Purdue University, West Lafayette, Indiana 47907, USA*

(Received 31 January 2009; accepted 12 June 2009; published online 6 August 2009)

We use molecular dynamics (MD) with the reactive interatomic potential ReaxFF to characterize the local strains of epitaxial Si/Ge/Si nanoscale bars as a function of their width and height. While the longitudinal strain (along the bars length) is independent of geometry, surface relaxation leads to transverse strain relaxation in the Ge section. This strain relaxation increases with increasing height of the Ge section and reduction in its width and is complete (i.e., zero transverse strain) for roughly square cross sections of Ge leading to a uniaxial strain state. Such strain state is desirable in some microelectronics applications. From the MD results, which are in excellent agreement with experiments, we derive a simple model to predict lateral strain as a function of geometry for this class of nanobars. © *2009 American Institute of Physics*. [DOI: 10.1063/1.3168424]

## I. INTRODUCTION

Strained heterostructures are ubiquitous in microelectronic and optoelectronic applications. Thin-body strained-Si and strained-Ge materials are attractive for metal-oxide-semiconductor field effect transistors (MOSFETs). In two-dimensional strained-Si channels, biaxial tensile strain enhances electron mobility by reshaping the band structures leading to a reduction in the electronic effective mass and the rate of intervalley phonon scattering;[1–3] consequently, such a structure is desirable for *n*-MOSFETs while the relatively low hole mobility enhancement limits its use for *p*-MOSFETs.[4] Buried $Si_{1-x}Ge_x$ channels grown on Si, which are compressively strained, exhibit enhanced hole mobility due to the reduction in intervalley scattering and the lack of $Si/SiO_2$ interface scattering.[1,5] The use of pure Ge ($x=0$) is attractive for *p*-MOSFETs because of the high hole mobility.[6,7] In recent years structures with nonhomogeneous in-plane strain states have attracted significant interest due to improved electronic properties.[1,6,8]

Accurate measurements of strain in nanostructures pose significant experimental challenges[6] and only average values are typically obtained; strain gradients, which can affect electronic properties, are hard to quantify. Atomic-level modeling and simulations can fill this gap and provide valuable information to help design and optimize strained-heterostructures.[9] In this paper we use molecular dynamics (MD) with an accurate, first-principles-based interatomic potential to characterize the local stresses in strained-Si/strained-Ge/strained-Si (s-Si/s-Ge/s-Si) nanobars as functions of the bar width and height of the Ge section ($H_{Ge}$); see Fig. 1 for a snapshot of one of our bars. We quantify the relaxation of lateral and vertical strains that occurs as the width of the bar is decreased or the height of the Ge section is increased. We find that the average strain state in the Ge section is approximately uniaxial (only along the axial direction) when the width of the bar is reduced to about $H_{Ge}$ section, i.e., for roughly square Ge cross sections.

This paper is organized as follows: Sec. II describes our computational approach including details of the atomistic models employed and interatomic potential. In Sec. III, we present the resulting strains as a function of bar geometry, and Sec. IVdiscusses the implications of our work. Finally, conclusions are drawn in Sec. V.

## II. SIMULATION DETAILS

### A. Atomistic models of s-Si/s-Ge/s-Si nanobars

Figure 1 shows a snapshot of one of our Si/Ge/Si nanobars. To build the heterostructures, we start with a diamond unit cell (eight-atom cubic cell) and replicate it along the *x*, *y*, and *z* directions to achieve the desired size of the bar. In all cases the cell is replicated six times along the *y* axis, which is the longitudinal direction of the bar, and periodic boundary conditions are imposed along this direction; this leads to [010] oriented nanobars. The number of unit cells in the *x* (transverse) and *z* (vertical) directions are varied to study the role of width and height on strain relaxation.

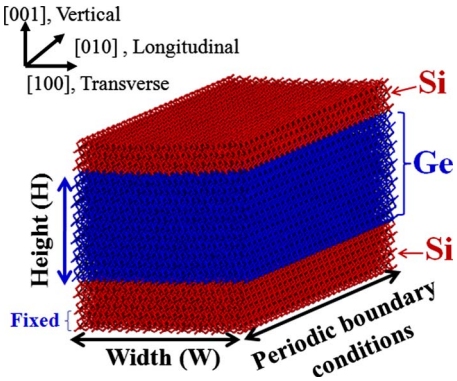


FIG. 1. (Color online) A snapshot of s-Si/s-Ge/s-Si nanobar oriented along [010].

[a)]Electronic mail: strachan@purdue.edu.

 

The lattice parameter in the $x$ and $y$ directions of the initial cell is 5.4284 Å (so initially Si is 2% in biaxial tension and Ge ~2% in biaxial compression). As shown in Fig. 1, the bottom three and top two unit cells along the vertical direction are made of Si atoms and the central region is Ge. The atomic positions of the bottom Si unit are kept fixed at the initial values to simulate the strong interaction of the bar with an oxide substrate. This setup leads to coherent structures with defect-free interfaces and is designed to reproduce bars fabricated by Hashemi *et al.*[6] using a bond and etch-back technique. Hashemi *et al.* grew the s-Si/s-Ge/s-Si heterostructure on relaxed SiGe virtual substrates. After bonding with the handling wafer, mechanical grinding and chemical processes are used to remove all its parts except the s-Si/s-Ge/s-Si on $SiO_2$ substrate. To study the effects of bar width, these structures are patterned into nanoscale gratings of different sizes using electron-beam lithography.[6,10] The resulting structures have the same orientation as our computational models.

### B. Interatomic potential: ReaxFF

We use the first-principles based interatomic potential ReaxFF[11] in our MD simulations. ReaxFF uses the concept of partial bond orders to model bond breaking and formation. It has been parametrized for Si using extensive *ab initio* simulations[12] and then extended.[13] We choose ReaxFF because it has been designed and parametrized to describe large strains including the process of bond breaking and formation, and consequently is expected to provide an accurate description of structures involving large deformations. This force field has been successfully used to describe crack propagation in Si (Ref. 13) and predict the structures of Si nanotubes.[14] In order to describe the interactions between Ge atoms, we make a simple extension of the Si force field where every distance parameter is increased by a factor of 1.0417; i.e., Ge is approximated as Si with a larger lattice parameter. Combination rules are used to calculate the Si–Ge covalent interactions and van der Waals cross interactions between Si and Ge atoms are described with Si parameters; the ReaxFF force field parameter file is included as supplementary material.[15]

In addition to ReaxFF, variety of many body interatomic potentials have been developed during the past decades for Si; the most widely used are the Stillinger–Webber (SW),[16] Tersoff,[17] environment dependent interatomic potential (EDIP),[18] and modified embedded atom models.[19,20] These potentials have been extensively applied to Si but a comprehensive study of their relative accuracy has not been carried out. SW has been reported to provide a more accurate description of reconstruction of (100) surfaces than Tersoff[21,22] and EDIP.[22]

Our choice of ReaxFF is based on the fact that it has been parametrized to describe large deformations including bond breaking and formation and its ability to describe oxides[12] and other material combinations. These features are critical for our future work that includes coherency limit calculations and passivated surfaces.

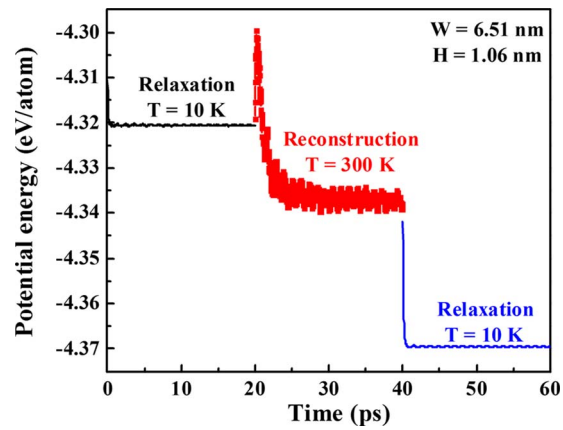


FIG. 2. (Color online) Potential energy vs time during MD procedure to find fully relaxed Si/Ge/Si. First MD runs at $T=10$ K under *NVT* conditions provide initial relaxation; $T=300$ K run enables surface atoms to reconstruct; final $T=10$ K relaxes the structure back to low temperature for more precise strain calculations.

### C. MD simulations: Structure relaxation and surface reconstruction

In order to produce fully relaxed structures for our wires, we use a procedure that consists of three steps (see Fig. 2): (i) First, we perform MD simulation using isothermal MD (*NVT* ensemble) for 20 ps at 10 K to relax the initial structures. (ii) We then increase temperature to 300 K and run an additional 20 ps of *NVT* dynamics. (iii) Finally, using the $T=300$ K structure, we decrease the temperature back to $T=10$ K and evolve the system an additional 20 ps. In all cases we use a time step of 0.5 fs to integrate the equations of motion. The initial $T=10$ K run relaxes the structure, but for such a low temperature we find that the surface does not reconstruct (only relaxation is observed). At $T=300$ K there is enough thermal energy for the surface to reconstruct and the final $T=10$ K run is used to remove thermal energy and produce structures that can be compared with those relaxed but not reconstructed surfaces. We used both the thermostats of Berendsen *et al.*[23] and Nose–Hoover[24] and, as expected, found no noticeable differences.

### D. Local strain calculations

To characterize the strain relaxation in our Si/Ge/Si bars, we compute local strain using the following approach. We calculate the distance between every pair of neighboring atoms and project it along the $x$, $y$, and $z$; based on these projections and using the corresponding values for the undeformed crystals (1.331 Å for Si and 1.386 Å for Ge), we calculate the bond strain. We compute the strain on each atom by averaging the associated bond strains. These are further averaged dividing the $x$-$y$ plane in square bins measuring $1.34\times1.34$ Å$^2$. This provides an accurate description, except for atoms on the surface that undergo large motion during reconstruction; such atomic rearrangement that involves the formation of new bonds and changes in topology cannot be described in terms of strain. Average strain on the Ge and Si sections is calculated from the atomic strains; only nonsurface atoms (i.e., those with four nearest neighbors) are considered for such averages.

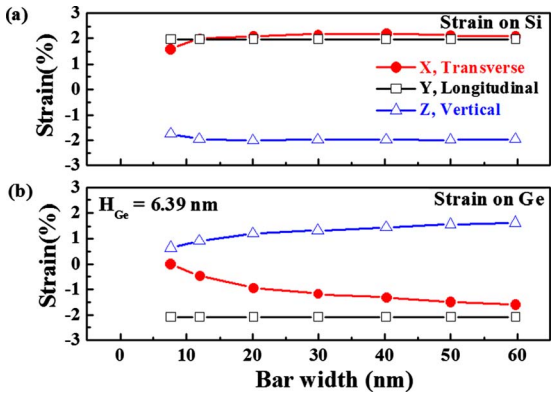


FIG. 3. (Color online) Average strains along the $x$, $y$, and $z$ axes for (a) Si and (b) Ge as a function of bar width for bars with Ge height $H_{Ge}$ =6.39 nm.

## III. RESULTS

### A. Role of bar width on strain relaxation

We fully relaxed and characterized the local strains of bars with widths from ~2 to ~60 nm and Ge sections with heights from ~1 to ~10 nm. We provide geometric details of all the bars as supplementary material.[15] Figure 3 shows the average strain of the Si and Ge sections as a function of width for bars with $H_{Ge}$=6.39 nm. Figure 4 shows the local strain maps on the bars' cross sections; the maps on the left [Figs. 4(a)–4(e)] show the transverse strain and those on the right [Figs. 4(f)–4(j)] show the local strains along the longitudinal direction. The local strain maps show both the Si and Ge sections; the Si top and bottom layers are in tension (and appear dark in the maps) and the Ge central region is in compression (and is denoted by a lighter color). Figure 3 shows that the strain along the longitudinal direction is independent of bar geometry and determined by the initial lattice parameter. Coherent epitaxial integration of Si and Ge and the fact that the bars are periodic in this direction (very long in the real material) precludes longitudinal strain relaxation. However, relaxation of (100) surfaces enables the Ge section

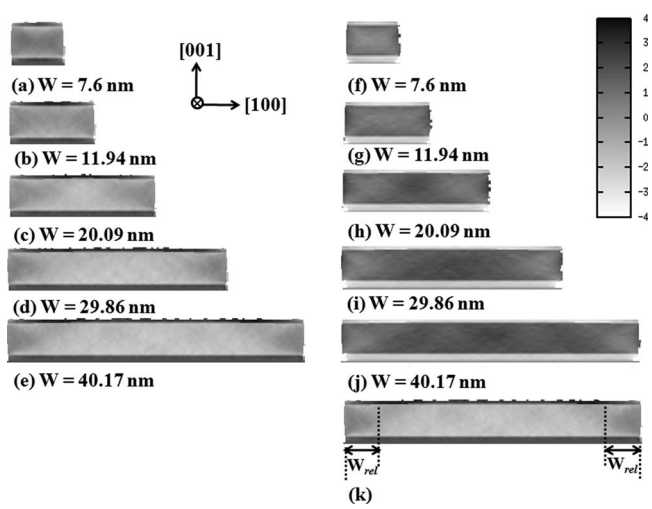


FIG. 4. Local strain maps over cross sections of bars with different widths but the same height of Ge ($H_{Ge}$=6.39 nm). Panels (a)-(e) and (f)–(j) show the transverse and longitudinal strains, respectively.

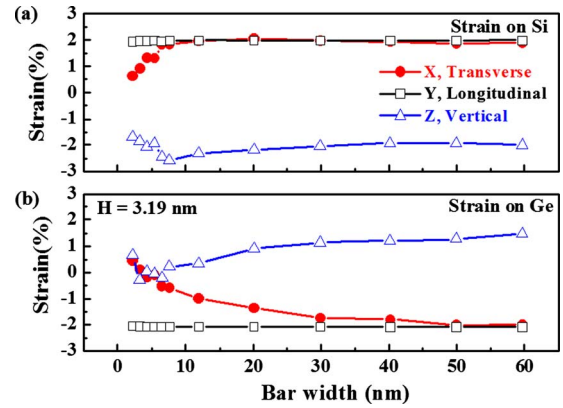


FIG. 5. (Color online) Average strains along $x$, $y$, and $z$ axes for (a) Si and (b) Ge as a function of the bar width for bars with Ge height $H_{Ge}$ =3.19 nm.

to expand laterally, leading to strain relaxation in the transverse direction. Regions of lateral strain relaxation can be seen in Figs. 4(a)–4(e) at the free (100) surfaces and appear darker than the central Ge region. These figures show that the extent of the regions that exhibit local strain relaxation is generally independent of bar width; figures with additional details on the size of the relaxation regions versus bar width are included in the supplementary material.[15] As the width of the bar is reduced, this relaxation plays an increasingly important role and the overall lateral strain of the Ge section decreases, see circles in Fig. 3. For bars with $H$=6.39 nm, we predict relatively little lateral relaxation (~23%) for a bar width of 60 nm (with an aspect ratio $W/H$~9.4); transverse strain relaxation increases to about 55% (strain of −1%) when the aspect ratio is reduced to $W/H$~3 (for $W$ =20 nm), and the lateral strain in Ge is essentially zero for an aspect ratio of 1. In the vertical direction, the Si and Ge sections are free to relax independently to zero stress. Figure 3 shows that Ge exhibits tensile strain in the vertical direction due to Poisson's effect and this vertical strain changes in response to the lateral relaxation. For bars with large widths, we can approximate the mechanical state of Ge as biaxial strain along the [100] and [010] directions ($\varepsilon_{xx}=\varepsilon_{yy}=-2.09\%$) and zero stress along the (vertical) [001] direction. Linear elasticity predicts $\varepsilon_{zz}=-4.18\nu/(1-\nu)=1.47\%$ for the Poisson ratio of our Ge description, $\nu$=0.260; [25] this number is in good agreement with the MD result even though large strains are involved. As the bar width and the lateral strain decrease, so does the vertical strain. For a bar with $W$ =7.60 nm, when the average lateral strain is roughly zero (and the longitudinal strain remains at 2.08%), the vertical strain is 0.64%.

Figure 5 shows average strains as a function of width, but for a bar with a thinner Ge section $H$=3.19 nm. Comparing Figs. 3 and 5, we see that strain relaxation is more pronounced in bars with thicker Ge sections. For the $H$ =3.19 nm bars, we find zero average transverse strain when the width is reduced to 3.26 nm (this number was 7.60 nm for $H$=6.39 nm).

### B. Role of Ge thickness on strain relaxation

Figure 6 shows how increasing the height of the Ge section for bars with width $W$=20.09 nm leads to transverse

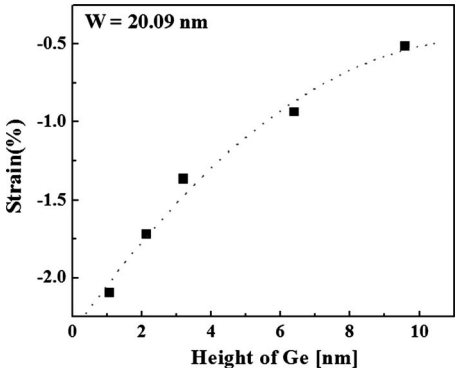


FIG. 6. Average transverse Ge strain as a function of height of Ge for bars with width $W=20.09$ nm. The dashed line is a guide to the eye.

strain relaxation in Ge. Figures 7(a)–7(d) display the corresponding local strain maps and show the role of Ge thickness on the area affected by lateral strain relaxation. As the Ge thickness is increased, the strain-relaxed area grows toward the center of the bar reducing the average Ge strain; the extension of the relaxation is more pronounced near the top Si layer than the bottom one where the atomic positions of the bottom third of the atoms are fixed to represent their interaction with the substrate.

### C. Role of surface reconstruction on strain relaxation

In order to quantify the role of surface reconstruction in the average strain relaxation in Ge, we compute strain for relaxed bars but without surface reconstruction. To this end we use the initial runs at 10 K where only surface relaxation is observed. Figure 8 shows the average strain in Ge for relaxed but not reconstructed (full squares) and reconstructed (open circles) surfaces as a function of width for two Ge heights. As shown in the Fig. 8, a significant fraction of strain relaxation occurs without surface reconstruction. For Si/Ge/Si nanobars with $H_{Ge}=6.39$ nm, surface reconstruction accounts for less than ~6% on total surface relaxation. However, surface reconstruction in thicker bars (with $H_{Ge}$

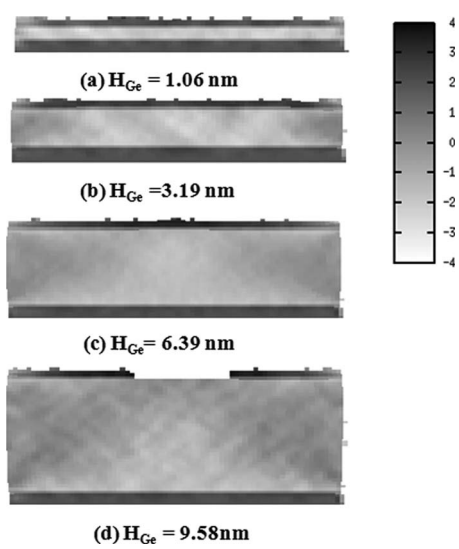


FIG. 7. Local strain maps over cross sections of bars with different Ge heights and the same width $W=20.09$ nm.

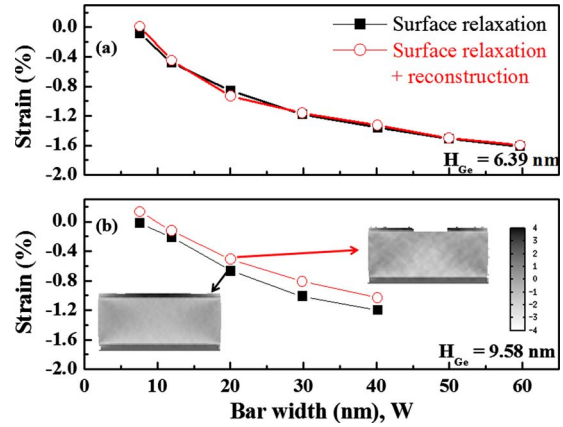


FIG. 8. (Color online) Average transverse Ge strain for relaxed but not reconstructed (full squares) and reconstructed (open circles) surfaces as a function of width for (a) $H_{Ge}=6.39$ nm and (b) $H_{Ge}=9.58$ nm. The insets show the local strain map of the Si/Ge/Si bar with $W=20.09$ nm and $H_{Ge}=9.58$ nm.

=9.58 nm) leads to an additional strain relaxation of up to ~16%. The local strain maps shown as insets of Fig. 8 show the origin of this enhanced relaxation. As the thin top Si layer reconstructs, it is able to further expand laterally releasing the strain of the top region of Ge. These results underscore the importance of an atomistic description in nanoscale device simulations where the details of surface processes can play a dominant role; note that finite element simulations in Ref. 6 underestimate the strain relaxation in Ge.

## IV. DISCUSSION

Figure 9 summarizes our results regarding average strain relaxation in the transverse direction as a function of width, for various heights. Here, the symbols represent data extracted directly from our MD simulations. We can see that for all cases significant lateral relaxation is obtained as the width of the bar is reduced to a value approximately equal to $H_{Ge}$ sections, i.e., bars with square cross sections exhibit close to uniaxial strain states. Our bar with width of 30 nm and Ge height of 6.4 nm is very similar in size to those built by Hashemi *et al.* and reported in Ref. 6. Using Raman spectroscopy, they estimated a 45% of transverse strain relaxation

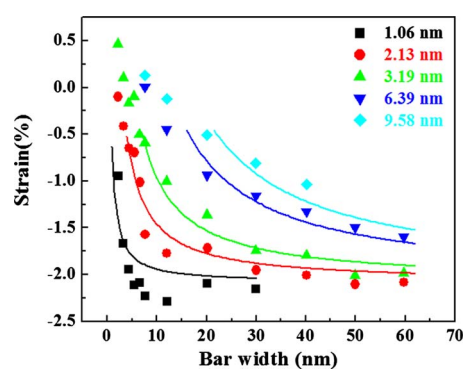


FIG. 9. (Color online) Average transverse Ge strain as a function of bar width for various Ge heights. The symbols represent data extracted from our MD simulations and the solid lines show our model [Eq. (2)] parametrized using the MD data.

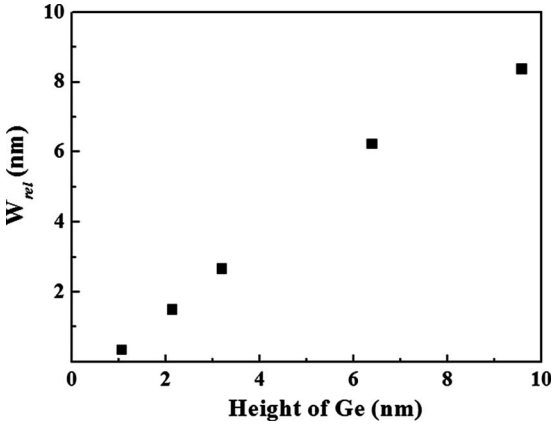


FIG. 10. Model parameter $W_{rel}$ obtained from fits to the MD data as a function of the height of the Ge section.

for that geometry; this number is in excellent agreement with our theoretical prediction of 44.5%, providing a very important validation to our predictions.

To model the dependence of average transverse strain on bar width, we divide the Ge section into three regions, as shown in the Fig. 4(k): a central one, far from the free (100) surfaces, with a local strain of 2.09% (given by the lattice parameter of the fixed Si layer) and two regions adjacent to the (100) free surfaces that exhibit strain relaxation. We can now write the average transverse engineering strain of Ge as

$$\langle \varepsilon \rangle = \frac{(1+0.0209)(W_0 - 2W_{\mathrm{rel}}) + (1+\varepsilon_{\mathrm{rel}}) \times 2W_{\mathrm{rel}} - W_0}{W_0}, \tag{1}$$

where $W_0$ is the strain-free width of the Ge section, $W_{\mathrm{rel}}$ is the width of each relaxed region, and $\varepsilon_{\mathrm{rel}}$ is their average strain. The first term of the numerator of the right hand side of Eq. (1) represents the width of the central region, the second one is the width of the two relaxed regions, and the engineering strain is calculated using its standard definition. We assume that the widths of the relaxed regions are independent of $W_0$ and further simplify our model (and reduce the number of free parameters) by taking $\varepsilon_{\mathrm{rel}}=0$ (this is equivalent to defining $W_{\mathrm{rel}}$ to a value such that the average strain of the relaxed regions is zero). With these simplifications, Eq. (1) reduces to

$$\langle \varepsilon \rangle = 0.0209 - 2 \times 0.0209 \frac{W_{\mathrm{rel}}}{W_0}, \tag{2}$$

with strain relaxation inversely proportional to the width of the bars. The solid lines in Fig. 9 show the proposed model [Eq. (2)] fitted to our MD data. Since the model is not expected to be valid for very small average strains, we only fit data with average strain $<-0.5\%$. Our simple model describes the MD well showing the largest discrepancies for very large relaxation or very thin Ge sections. The fitted parameter $W_{\mathrm{rel}}$ is shown as a function of $H_{\mathrm{Ge}}$ in Fig. 10; as expected $W_{\mathrm{rel}}$ increases with the height of Ge and its numerical value is very similar to $H_{\mathrm{Ge}}$. Thus, approximating $W_{\mathrm{rel}}$ as $H_{\mathrm{Ge}}$, we obtain a parameter-free model to estimate strain relaxation in Si/Ge/Si heterostructures. Our simple model overestimates strain relaxation for bars with small widths but it could be a useful to provide initial estimates in device design and optimization.

## V. CONCLUSIONS

We studied strain relaxation in epitaxial Si/Ge/Si heterostructures, which are good candidates for channel material for *p*-MOSFETs, using MD simulations. We characterize how surface relaxation leads to transverse strain relaxation as a function of geometry. Our simulations show that the lateral strain in the Ge section is relaxed as the bar width is reduced or the Ge height is increased. Approximately uniaxial strain occurs for bars with square Ge cross sections. Our results show large strain gradients in the nanostructures that could have an important effect on their electronic response; we are currently investigating these effects. Based on our extensive MD results (in excellent agreement with experiments), we derived a simple model to estimate the average strain in this class of heterostructures that could be useful in early device design or optimization processes. All our structures exhibit coherent, defect-free interfaces; the presence of interfacial dislocations will lead to additional strain relaxation and we are currently investigating their effect.

## ACKNOWLEDGMENTS

This work was supported by the Microelectronics Advanced Research Corporation and its Focus Center on Materials, Structures and Devices, by the Network for Computational Nanotechnology through nanoHUB.org computational resources funded by the U.S. National Science Foundation Grant No. EEC-0228390.

[1] I. Aberg, C. Cait Ni, and J. L. Hoyt, IEEE Trans. Electron Devices **53**, 1021 (2006).
[2] M. L. Lee, E. A. Fitzgerald, M. T. Bulsara, M. T. Currie, and A. Lochtefeld, J. Appl. Phys. **97**, 011101 (2005).
[3] V. Vartanian, S. Zollner, A. V.-Y. Thean, T. White, B.-Y. Nguyen, L. Prabhu, D. Eades, S. Parsons, H. Desjardins, K. Kim, Z.-X. Jiang, V. Dhandapani, J. Hildreth, R. Powers, G. Spencer, N. Ramani, M. Kottke, M. Canonico, X.-D. Wang, L. Contreras, D. Theodore, R. Gregory, and S. Venkatesan, IEEE Trans. Semicond. Manuf. **19**, 381 (2006).
[4] C. W. Leitz, M. T. Currie, M. L. Lee, Z. Y. Cheng, D. A. Antoniadis, and E. A. Fitzgerald, Appl. Phys. Lett. **79**, 4246 (2001).
[5] M. Willander and S. C. Jain, *Silicon-Germanium Strained Layers and Heterostructures* (academic, New York, 2003), pp. 195–201.
[6] P. Hashemi, L. Gomez, J. L. Hoyt, M. D. Robertson, and M. Canonico, Appl. Phys. Lett. **91**, 083109 (2007).
[7] M. L. Lee and E. A. Fitzgerald, Appl. Phys. Lett. **83**, 4202 (2003).
[8] R. Z. Lei, W. Tsai, I. Aberg, T. B. O'Reilly, J. L. Hoyt, D. A. Antoniadis, H. I. Smith, A. J. Paul, M. L. Green, J. Li, and R. Hull, Appl. Phys. Lett. **87**, 251926 (2005).
[9] A. Arumbakkam, E. Davidson, and A. Strachan, Nanotechnology **18**, 345705 (2007).
[10] L. Gomez, M. Canonico, M. Kim, P. Hashemi, and J. L. Hoyt, J. Electron. Mater. **37**, 240 (2008).
[11] A. C. T. van Duin, S. Dasgupta, F. Lorant, and W. A. Goddard III, J. Phys. Chem. A **105**, 9396 (2001).
[12] A. C. T. van Duin, A. Strachan, S. Stewman, Q. Zhang, X. Xu, and W. A. Goddard III, J. Phys. Chem. A **107**, 3803 (2003).
[13] M. J. Buehler, A. C. T. van Duin, and W. A. Goddard, Phys. Rev. Lett. **96**, 095505 (2006).
[14] A. Palaria, G. Klimeck, and A. Strachan, Phys. Rev. B **78**, 205315 (2008).
[15] See EPAPS supplementary material at 10.1063/1.3168424 for the ReaxFF force field parameter file.
[16] F. H. Stillinger and T. A. Weber, Phys. Rev. B **31**, 5262 (1985).

[17]J. Tersoff, Phys. Rev. B **38**, 9902 (1988).
[18]N. Bernstein, M. J. Aziz, and E. Kaxiras, Phys. Rev. B **61**, 6696 (2000).
[19]M. I. Baskes, Phys. Rev. B **46**, 2727 (1992).
[20]J. G. Swadener and S. T. Picraux, J. Appl. Phys. **105**, 044310 (2009).
[21]L. Nurminen, F. Tavazza, D. P. Landau, A. Kuronen, and K. Kaski, Phys. Rev. B **67**, 035405 (2003).
[22]J. Godet, L. Pizzagalli, S. Brochard, and P. Beauchamp, J. Phys.: Condens. Matter **15**, 6943 (2003).
[23]H. J. C. Berendsen, J. P. M. Postma, W. F. van Gunsteren, A. Di Nola, and J. R. Haak, J. Chem. Phys. **81**, 3684 (1984).
[24]W. G. Hoover, Phys. Rev. A **31**, 1695 (1985).
[25]J. J. Wortman and R. A. Evans, J. Appl. Phys. **36**, 153 (1965).